IEEE Access
Multidisciplinary | Rapid Review | Open Access Journal

Received April 11, 2021, accepted April 23, 2021, date of publication April 28, 2021, date of current version May 4, 2021.

Digital Object Identifier 10.1109/ACCESS.2021.3076260

Analysis and Design of Novel Structured High Torque Density Magnetic-Geared Permanent Magnet Machine

SOHEIL YOUSEFNEJAD[1], HOSSEIN HEYDARI[1], KAN AKATSU[2], AND JONGSUK RO[3,4]

[1]Department of Electrical Engineering, Iran University of Science and Technology, Tehran 16846-13114, Iran
[2]Division of Intelligent Systems Engineering, Faculty of Engineering, Yokohama National University, Yokohama 240-8501, Japan
[3]School of Electrical and Electronics Engineering, Chung-Ang University, Seoul 06974, South Korea
[4]Department of Intelligent Energy and Industry (BK4), Chung-Ang University, Seoul 06974, South Korea

Corresponding author: Jongsuk Ro (jongsukro@gmail.com)

This work was supported in part by the Basic Science Research Program through the National Research Foundation of Korea by the Ministry of Education under Grant 2016R1D1A1B01008058, and in part by the Human Resources Development of the Korea Institute of Energy Technology Evaluation and Planning (KETEP) Grant by the Korean Government through the Ministry of Trade, Industry and Energy under Grant 20184030202070.

ABSTRACT The main limitation of magnetic gears is their relatively low torque density. Therefore, a novel structured high torque density magnetic-geared permanent magnet (MGPM) machine, which combines the advantages of a conventional MGPM machine and magnetic gear to enhance the torque considerably and achieve low-speed high-torque operation, is proposed in this study. However, there are different structures for increasing torque of a machine. Therefore, in order to demonstrate the advantages of the proposed structure, it is compared with other structures, using the finite element method. Moreover, the proposed MGPM machine can transmit an additional 42.3% of torque density when compared with the conventional MGPM machine of the same size.

INDEX TERMS Bi-directional flux modulating, bread-loaf shaped permanent magnet, dual-layer permanent magnet excitations, electrical continuously variable transmission (E-CVT), Halbach permanent magnet arrays, MGPM machine, torque density.

I. INTRODUCTION

Gearboxes play an important role in different industries, as a transferring torque from input to output side [1]. Despite having several merits, such as high torque density, the mechanical gears have some limitations [2]. One of the main limitations is that substantial frictional forces in mechanical gears are produced between meshing teeth, which leads to wear and breakage. Furthermore, disadvantages, such as need for lubrication and cooling, low life expectancy, low efficiency, and large dimensions have led to a new approach for gearboxes [3]–[5]. This new approach employs magnetic materials on the structure of the gears, which is called ''magnetic gear'' [6]–[8].

In general, the rudimentary magnetic gear topologies originate from mechanical gear topologies. In this way, the slots and teeth in the mechanical gears are replaced with the N and S poles of the permanent magnet (PM) in magnetic gears, respectively [9], [10]. In all magnetic gears, the torque is transmitted via interaction of modulated magnetic fields instead of mechanical teeth [11], [12]. Moreover, the magnetic gears have advantages, such as physical isolation between input and output shaft, low noise, maintenance free, high reliability, and inherent overload protection, which plays an important role in wind turbines during a storm [6], [13]–[16]. Therefore, magnetic gears improve reliability and reduce maintenance costs.

In spite of their advantages over mechanical gears, magnetic gears have some disadvantages. In general, the biggest issue of the magnetic gears is the torque density. Therefore, studies [17]–[24] proposed various structures in order to increase the torque.

First, one of the structures integrates the magnetic gear with the PM brushless motor, which increases the torque density. The inner rotor of the magnetic gear is removed, and it benefits from the stator winding instead of the inner rotor;

The associate editor coordinating the review of this manuscript and approving it for publication was Agustin Leobardo Herrera-May.

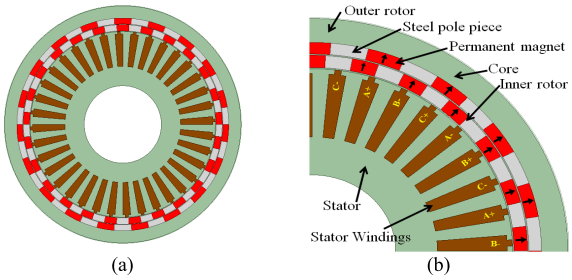

FIGURE 1. Structure of DL-MGPM machine.

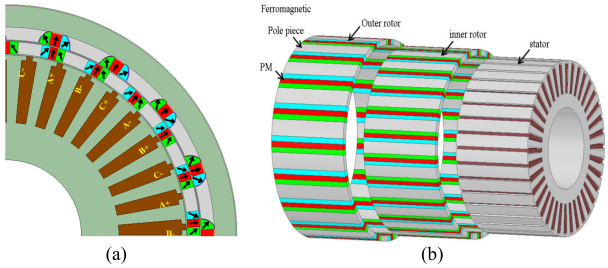

FIGURE 2. Structure of MGPM: (a) HDL-MGPM (b) 3D illustration of HDL-MGPM.

this structure is referred to as the magnetic-geared permanent magnet (MGPM) machine [20], [25], [26]. In addition, this structure reduces the dimensions and the overall weight of the magnetic gear [27]. Second, torque density can be increased by insertion of the PMs inside the rotor, which is referred to as the interior permanent magnet (IPM) [28]–[32]. In addition, the other way of enhancement of the torque density is to change magnetization directions of PMs based on the Halbach PM arrays [33]–[35]. This structure increases the torque density and reduces torque ripple [17], [36, [37]. Finally, torque density can be increased by employing the PMs on both the inner and outer rotors; this structure is referred to as the dual layer-MGPM (DL-MGPM) machine [38], [39]. As shown in Fig. 1, in the DL-MGPM machine, PMs on both rotors have the same mag-netization directions. In this structure, a stronger coupling of the magnetic field between the rotor PMs and the current of armature is engendered, which leads to increasing torque density. However, this structure has high torque ripple, which is a major disadvantage of the structure [40].

Therefore, to address this problem, a useful structured MGPM machine is proposed in this study. The proposed structure overcomes the drawbacks of the previous structures and can achieve low-speed high-torque operation. Furthermore, the electric continuous variable transmission system (E-CVT) can be achieved with the proposed structure, which is useful in a broad spectrum of industry and application [41], such as hybrid electric vehicles (HEVs) [42]–[44] and marine [45].

The purpose of this study is to propose a novel structure of MGPM machine based on the professional integration of the three topologies of the Halbach PM arrays, the dual-layer PM excitations, and Bread-Loaf-shaped PM. By applying these structures, the waveform of the magnetic field becomes closer to the sinusoidal wave, resulting in a stronger and more effective coupling between the generated magnetic fields. Subsequently, the proposed structure considerably enhances the torque density and decreases torque ripple.

II. GENERAL TOPOLOGY OF NOVEL STRUCTURE OF MGPM MACHINE

The proposed structure combines the advantages of Halbach PM arrays, the Bread-Loaf shaped PM, and the DL-MGPM machine, which is referred to as the Halbach PM arrays dual layer-MGPM (HDL-MGPM) machine. This structure and its 3D view are shown in Fig. 2(a) and 2(b), respectively.

A. STRUCTURE OF THE DL-MGPM MACHINE

As shown in Fig. 3(a), the PMs and steel pole pieces of this structure are placed in the rotors next to one another, which create the PM-steel pole piece array. This structure causes the inner rotor to create two types of magnetic fields in the inner and outer air gap via inner rotor PMs and steel pole pieces, simultaneously: modulated magnetic field via inner rotor steel pole pieces and excited magnetic field via inner rotor PMs. Thus, the outer rotor has this PM-steel pole piece array. Then, this array acts similar to the inner rotor array. Therefore, both the inner and outer rotors modulate the magnetic fields simultaneously, which is called bi-directional flux modulating effect. Moreover, the bi-directional flux modulating effect leads to strong coupling between the magnetic fields in the air gaps [40].

B. STRUCTURE OF THE HALBACH PM ARRAYS

As shown in Fig. 3(b), the magnetic fluxes are concentrated on one side, even though the magnetic fluxes in the other side are dispersed. Hence, the Halbach PM array augments the magnetic fields in the air gaps and reduces the strength of magnetic fields in the core of the rotor. This structure increases torque density and decreases the torque ripple drastically [17].

C. BREAD- LOAF-SHAPED PM MODEL

As shown in Fig. 3(c), the shape of the PMs is changed; the thickness of the edges of the PMs is reduced. This structure reduces the torque ripple and peak cogging torque. Furthermore, the peak back-emf remains approximately constant [46]–[49].

In the dual-layer PM excitations, rotor steel pole pieces modulate the magnetic fields as follows [40]:

1) First, the inner rotor steel pole pieces modulate the generated magnetic fields of the rotors and stator in the inner and outer air gap.

2) Second, the outer rotor steel pole pieces modulate the generated magnetic fields of the rotors in the outer air gap. Finally, the bi-directional flux modulating effect produces

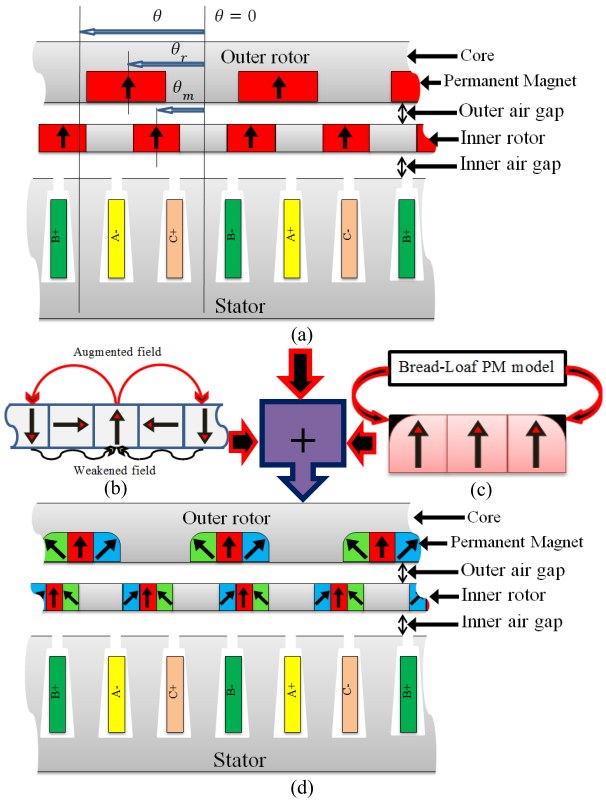

FIGURE 3. Structure of MGPM machines and novel structure (a) dual-layer PM excitations (b) Halbach PM arrays (c) Bread-Loaf-shaped PM (d) the proposed novel MGPM machine.

a strong coupling between the magnetic fields of outer and inner rotor and inner stator.

Therefore, in the proposed structure, there are 2 strength types of the magnetic field: enhanced and reduced magnetic fields in the air gaps.

1) Enhanced magnetic fields in the air gaps

There are three reasons for this phenomenon and they are explained as follows:

a) As shown in Fig. 3(d), by changing the magnetization directions of the outer rotor PMs similar to Halbach PM arrays, it is expected that the magnetic fields in the outer air gap is enhanced. However, the magnetic fields in the outer rotor core are reduced. These weakened magnetic fields lead to the selection of a core with less width for outer rotor.

b) PM magnetization directions in the inner rotor are arranged as Halbach PM arrays in order to enhance the magnetic field in the outer air gap. Furthermore, these enhanced magnetic fields are modulated by the outer rotor steel pole pieces in order to induce the effective magnetic field in the outer air gap owing to the bi-directional flux modulating effect.

c) In the outer rotor, the Bread-Loaf shaped PM plays a role similar to Halbach PM arrays. As shown in Fig. 3(c), edges of PM sections are clipped. The Bread-Loaf shaped PM causes enhancement of the magnetic fields in the outer air gap and decreases the magnetic fields in the outer rotor core. Moreover, the Bread-Loaf shaped PM can decrease the torque ripple since the magnetic fields in the outer air gap are more sinusoidal.

2) Reduced magnetic fields in the outer rotor core and the inner air gap

In the inner air gap, the magnetic fields created by inner rotor PMs are decreased in the inner air gap via the Halbach PM array, since the harmonic order of the magnetic fields has low impact on torque density. These weakened magnetic fields are artfully chosen in this structure in order to decrease torque ripple considerably. These reduced magnetic fields are another novelty of the proposed structure. Furthermore, the Bread-Loaf-shaped PM is employed on the outer rotor PMs. Then, the strength of magnetic flux toward the outer rotor core is decreased. Therefore, this change in the shape of PM decreases torque ripple and decreases the probability of saturation in the cores.

III. WORKING PRINCIPLE OF PROPOSED MGPM MACHINE

In this study, the proposed structure improves the effects of magnetic fields in the air gaps in order to increase the torque density and decrease the torque ripple. Moreover, magnetic fluxes in the outer air gap are augmented and the magnetic fluxes in the inner air gap are decreased, in order to improve the effects of magnetic fields in the air gaps. These changes in the magnetic fluxes in the air gaps are achievable via Halbach PM array. In contrast, the magnetic fields in the outer rotor core are reduced via Bread-Loaf-shaped PM in order to decrease the torque ripple.

A. PROPOSED DESIGN FLOW CHART FOR MGPM MACHINES

The design flowchart for MGPM machines is proposed in Fig. 4.

Step1: Determination of design specifications

In the magnetic gears, the fundamental harmonics of magnetic fields in the air gaps play the main role in producing torque. Similarly, other harmonics of magnetic fields in the air gaps cause negative effects, such as increasing torque ripple, speed fluctuations, and vibrations. In this study, the novel structure of MGPM is proposed, which will be a suitable alternative to gears in a wide spectrum of industries. For a fair comparison, the simulation models are executed with the same specification, such as that of the total PM volume, overall radius, and air gap length. In other words, only the structures of the PMs in these machines are changed. Because the magnetic energy is related to the volume of the PM, in this study, the total volume of PMs through the comparison of the MGPM machines is considered constant. Subsequently, according to the equal total volume of machines, the volume of steel in these machines can be calculated.

Step2: Determination of core material Silicon Steels are the most popular materials in machinery industries. Therefore, these silicon steels are available in an array of grades and thicknesses, such as M19, M27, M36, and M43. In these

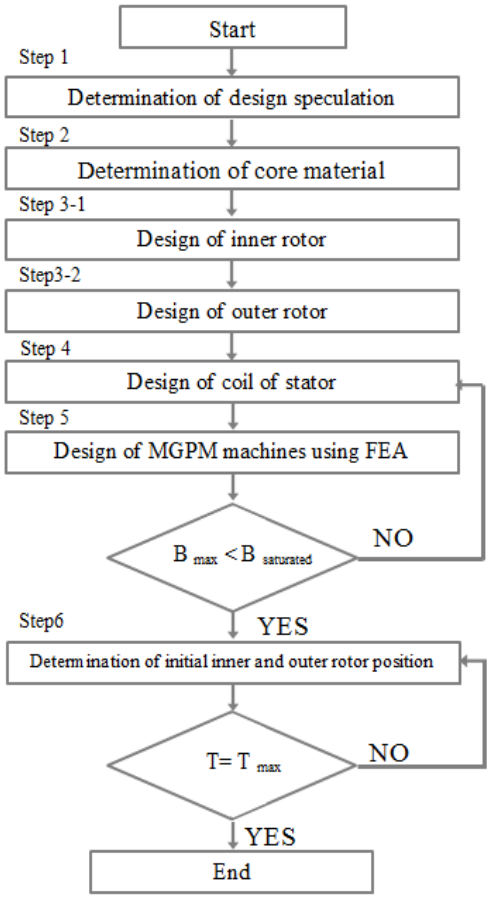

FIGURE 4. Proposed design flow chart for MGPM machine.

grades, order of maximum core loss has direct relation to M numbers. Despite the core loss being increased by increase in M numbers, the cost of core material is decreased. Therefore, M43 material core is chosen for MGPM machines in this study in order to decrease the cost of the machines. Furthermore, in order to obtain complete advantage of a laminated core, the laminations should be insulated from each other.

Step3: Design of the rotors The MGPM machine consists of one stator and the inner and outer rotors.

Therefore, the design of these MGPM machines is implemented based on following equations[50]:

$$\begin{cases} P_{m,k} = |mP + kN_s| \\ m = 1, 3, 5, \ldots, \infty \\ k = 0, \pm 1, \pm 2, \ldots, \pm\infty \end{cases} \tag{1}$$

where Pm,k is the number of pole-pairs in the space harmonic flux density distribution and P is the number of pole pairs of the permanent magnet; m and k represent the orders of the space harmonic and N_s is the number of ferromagnetic pole pieces in the inner rotor.

The relationship between the number of pole pairs is presented as follows: [11].

$$N_s = P_s + P_r \tag{2}$$

where, P_r and P_s are the number of pole pairs of outer rotor and stator, respectively. In this study, the parameters are $P_s = 6$, $P_r = 19$, $N_s = 25$. The relationship between speeds is as follows [11]:

$$\Omega_r(m,k) = \frac{mP_s}{mP_s + kN_s}\Omega_s + \frac{kN_s}{mP_s + kN_s}\Omega_{ml} \tag{3}$$

where Ω_r, Ω_{ml}, and Ω_s are the speed of the outer rotor, speed of the inner rotor, and rotating speed of magnetic field of the stator winding current, respectively. If the inner rotor is stationary, the gear ratio is expressed as follows [51]:

$$N(m,k) = \frac{mP_s + kN_s}{mP_s} \tag{4}$$

The relationship between the mechanical rotating frequency of the motor (F) and the stator frequency (f) can be expressed as follows [11]:

$$f = F.P_r/P_s \tag{5}$$

Step 3-1: Design of inner rotor In the conventional MGPM machine, there are only steel pole-pieces in the inner rotor owing to the magnetic field modulation. In the inner rotor of the proposed structure, PMs and steel pole pieces are placed close together and create an array of PMs-steel pole pieces.

In this study, the radius of the inner rotor of the MGPM machines is selected based on higher torque. Furthermore, for fair comparison, the total PM volume is assumed to be 484 cm^3. Therefore, this condition must be satisfied in the proposed structure. In the other words, the PM volume of inner and outer rotor must be optimized.

The fundamental component of the magneto motive force (MMF) of the PM is as follows [52]:

$$F_{PM}(\theta) \approx F_{PM1}\cos P_r(\theta - \theta_r) \tag{6}$$

where, F_{PM1} is the amplitude of the fundamental component of the MMF of the PM, θ and θ_r are the mechanical angels on the stator and the rotor position, respectively [52].

The air gap permeance coefficient in the magnetic geared-PM machines can be expressed as [52]:

$$P(\theta) \approx P_0 + P_1\cos N_s(\theta - \theta_m) \tag{7}$$

where, P_0 and P_1 are the zero- and first order harmonics of the air gap permeance coefficient, respectively, θ_m is the modulation layer position. In the (7), the saturation of the steel pole pieces and magnetic resistance are neglected.

By neglecting the higher order component than P_r, the flux density of the open circuit air gap is expressed as:

$$\begin{aligned} B_{PM}(\theta) &= F_{PM}(\theta)P(\theta) \\ &\approx B_{PM0}\cos P_r(\theta - \theta_r) \\ &\quad + B_{PM1}\cos[(P_r - N_s)\theta - P_r\theta_r + N_s\theta_m] \end{aligned} \tag{8}$$

where,

$$B_{PM1} = \left(\frac{F_{PM1}P_1}{2}\right) \tag{9}$$

$$B_{PM0} = F_{PM1}P_0 \tag{10}$$

The inner rotor torque is expressed via following equations [52]:

$$T_{ir} = +(\frac{\pi}{2\sqrt{2}})k_{w1}A(\frac{P_r}{P_s})B_{pm1}D_l^2L_{stack} \quad (11)$$

where,

$$A = (\frac{6}{\pi D_l})N_{ts}I_{ph} \quad (12)$$

where, A is the electric loading, N_{ts} is the number of the series turns of winding, I_{ph} is the root mean square (RMS) value of the current of per phase, D_l is the outer diameter of inner stator, and k_{w1} is the fundamental winding factor and L_{stack} is the length of the lamination [52].

Step3-2: Design of outer rotor The thickness of outer rotor PMs and radius of the outer rotor are justified to produce higher torque and even prevent core saturation. In the proposed structure, the outer rotor is similar to the inner rotor; the outer rotor consists of PMs and steel pole pieces, which are placed next to each other in an array. Hence, the calculation of the outer rotor PM volume is similar to that of the inner rotor. The outer rotor torque is expressed by following equation [52]:

$$T_{or} = -(\frac{\pi}{2\sqrt{2}})k_{w1}A(\frac{N_{ts}}{P_s})B_{pm1}D_l^2L_{stack} \quad (13)$$

Step4: Design of coil of stator In this study, the torque of the machines is controlled via coil current, according to (8) and (9). As expressed in (8) and (9), torques of the MGPM machines has a direct relation with the amplitude of current of the stator. Furthermore, these equations are combined to form the following equation:

$$\frac{T_{or}}{T_{ir}} = -\frac{N_s}{P_r} \quad (14)$$

Therefore, it is shown that the torque of the inner rotor and the outer rotor are related. Hence, torques of the MGPM machine can be controlled by changing the amplitude of current. In addition, the currents of the coil of stator create the required magnetic fields in the inner air gap in order to produce the torques. In this step, after changing current of the stator, the rule of Bmax>Bsaturated should be satisfied for all segments of the machines such as inner and outer rotor and stator core.

1) Step5: Design of MGPM machines using FEA

All MGPM machines are simulated in the Ansys software, and the resulting data are analyzed using the MATLAB software.

2) Step6: Determination of initial outer rotor position

In general, the MGPM machines must supply the torque of the load in steady state. Thereafter, the torque in the steady state can operate near maximum. Therefore, in order to achieve this torque in the simulation, the initial position of the rotors should be determined.

B. MAGNETIC FIELDS IN THE MGPM MACHINES

In general, the magnetic fields play a vital role in magnetic gears. In these machines, magnetic fields in the air gaps interact with each other in order to produce torque. The torque of the inner and outer rotor of the machines as a function of magnetic fields is calculated as follows [17]:

$$T_{ir} = (\frac{L_{stack}R_{in}^2}{\mu_0})\int_0^{2\pi} B_{rin}B_{\theta in}d\theta \quad (15)$$

$$T_{or} = (\frac{L_{stack}R_{out}^2}{\mu_0})\int_0^{2\pi} B_{rout}B_{\theta out}d\theta \quad (16)$$

where R_{in} and R_{out} are radius of inner and outer air gap, respectively. As illustrated in [17], it can be found that the flux densities in the air gaps are the sum of infinite harmonic terms. Each term of the flux densities in the certain current value are expressed as follows:

$$B_{rin} = \delta_i \cos(P_m\theta + \alpha) \quad (17)$$

$$B_{\theta in} = \varepsilon_i \sin(P_n\theta + \beta) \quad (18)$$

$$B_{rout} = \gamma_i \cos(P_m\theta + \alpha) \quad (19)$$

$$B_{\theta in} = \zeta_i \sin(P_n\theta + \beta) \quad (20)$$

where P_m and P_n are the spatial harmonic component of the radial and tangential flux density, respectively, δ_i, ε_i, γ_i and ζ_i are the coefficients which depend on the current value, and α and β are the phase angles of the magnetic field. By combining (17) and (18) in (15), the following expression can be derived [17]:

$$\begin{cases} T_{ir} = \delta_i\varepsilon_i\pi \sin(\beta - \alpha) & P_n = P_m \\ T_{ir} = 0 & P_n \neq P_m \end{cases} \quad (21)$$

Similarly, the outer rotor torque is similar to (21). Thus, the same magnetic field harmonic component can produce torque.

IV. MAGNETIC FIELDS HARMONIC ANALYSIS OF NOVEL STRUCTURE

Radial flux density of the inner and outer air gap of DL-MGPM and HDL-MGPM are shown in Fig. 5 and 6, respectively. In these figures, the magnetic field is produced by the stator windings and PMs, which are placed in the inner and outer rotors.

As shown in Fig. 5, in the proposed structure, the 6^{th} harmonic component of Flux Density in the inner air gap is effective since it is the main harmonic. Thereafter, this harmonic component is augmented via employing the Halbach PM array on the outer rotor PMs, such that their magnetic fluxes are concentrated toward the inner air gap. These magnetic fluxes are modulated by the inner rotor steel pole pieces. Thereafter, the magnetic fluxes via 6^{th} harmonic component are created in the inner air gap.

Thus, the augmented magnetic fluxes which are produced by outer rotor PMs enhance the magnetic fluxes in the inner air gap. Therefore, the flux of the inner rotor PMs is modulated via both outer and inner steel pole pieces. Furthermore,

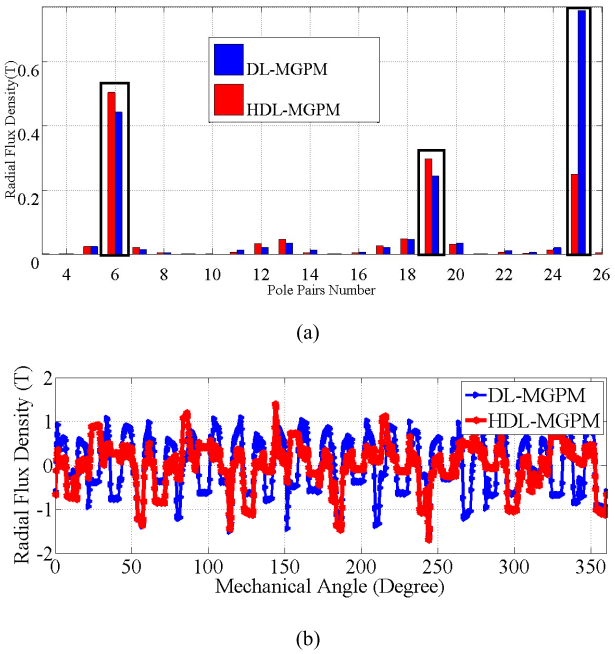

FIGURE 5. Radial flux densities of DL-MGPM and HDL-MGPM in the inner air gap.

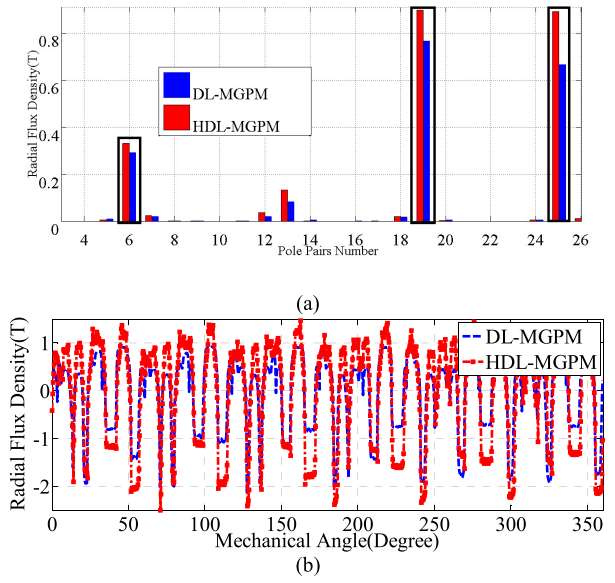

FIGURE 6. Radial flux densities of DL-MGPM machine and HDL-MGPM machine in the outer air gap.

the 19th harmonic component of magnetic flux in the inner air gap is augmented.

In contrast, the amplitude of 25th harmonic component of the magnetic flux is decreased considerably because of applying Halbach PM array in the inner rotor PMs, where the magnetic fluxes are dissipated in the inner air gap, although they are focused in the outer air gap.

As shown in Fig. 6, in the proposed structure, the 6th, 19th, and 25th harmonic components of the magnetic flux are augmented since magnetization directions of the inner and

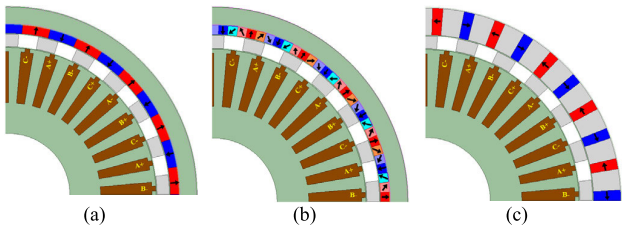

FIGURE 7. MGPM machines: (a) CSL- MGPM (b) HSL-MGPM (c) IPMSL-MGPM.

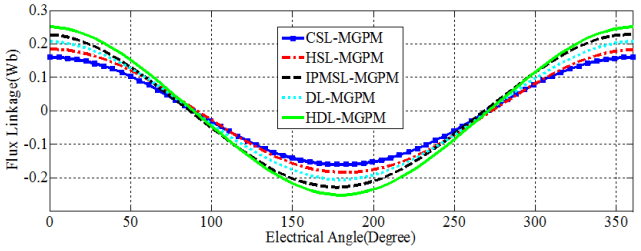

FIGURE 8. Flux linkage waveforms.

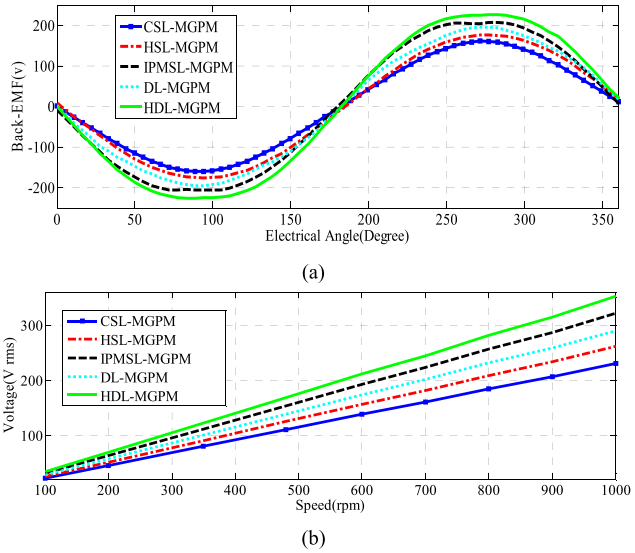

FIGURE 9. Induced back-EMF waveforms: (a) With outer rotor at 480 rpm (b) with outer rotor at different speed.

outer rotor PMs are arranged based on Halbach PM array in order to concentrate the magnetic fluxes in the outer air gap. In the outer air gap, the 19th and 25th harmonic components are useful and effective in producing torque.

Therefore, the magnetic fluxes in the proposed structure are improved in the air gaps in order to produce higher torque compared to other MGPM machines.

V. PARAMETERS OF THE MGPM MACHINES

In order to demonstrate the superiority of the proposed structure, a quantitative comparison of the proposed structure with the DL-MGPM, conventional single-layer MGPM (CSL-MGPM) [8], Halbach PM arrays single-layer MGPM

TABLE 1. Design Parameters.

	CSL-MGPM	HSL-MGPM	IPMSL-MGPM	DL-MGPM	HDL-MGPM
Overall radius	122.5 mm				
Axial length	120 mm				
Air gap length	0.7 mm				
Thickness of outer rotor PM	5.93 mm		17.1 mm	6 mm	
Rotor PM ratio	50 %		33 %	50 %	
Thickness of inner rotor	8 mm			6.43 mm	
No. of phase	3				
No. of stator pole-pairs	6				
No. of outer rotor pole-pairs	19				
No. of ferromagnetic segments	25				
No. of conductors Turns	25				
Remanence of the PMs	1.1[T]				
PM Relative permeability	1.0446				
Core material	M43-29G				
PM material	NdFeB				
Total PM volume	0.000484 m^3				
Total copper volume	0.000582 m^3				
Core weight (Kg)	24.30			26.648	
Copper weight (Kg)	8.963				
Total weight (Kg)	36.92			39.268	
Motor Volume ($cm3$)	4644.03			4948.54	

(HSL-MGPM), and IPM single-layer MGPM (IPMSL-MGPM) is performed. The Figs. 7(a), 7(b), and 7(c) show the CSL-MGPM, the HSL-MGPM, and the IPMSL-MGPM, re-spectively.

For fair comparison, the overall radius of the MGPM machines, axial stack length, and the PM and copper volume are supposed to be constant for all machines. The major parameters of these MGPM machines are listed in Table 1.

VI. COMPARISON OF DESIGNS

The comparisons are performed assuming the outer rotor rotates at 480 rpm. In this case, the flux linkages and no load back-EMF are shown in Figs. 8 and 9, respectively. As shown in Figures 8 and 9, the flux linkages and no load Back-EMF are close to sinusoidal waveform; the proposed structure has the highest value, and CSL-MGPM has the lowest one.

The frequency of the induced voltage and the flux linkage is 152 Hz, which can be calculated from (5). It is shown that the RMS value of the back-EMF of the proposed structure,

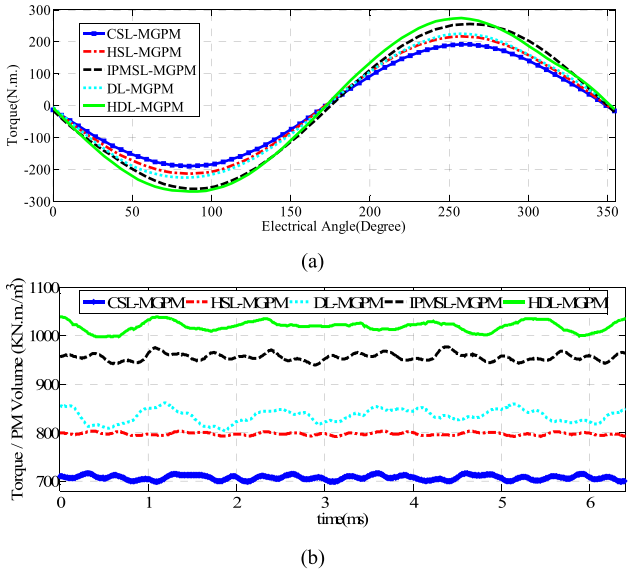

FIGURE 10. Electromagnetic torque waveforms of outer rotor: (a) Torque–angle curves (b) steady state.

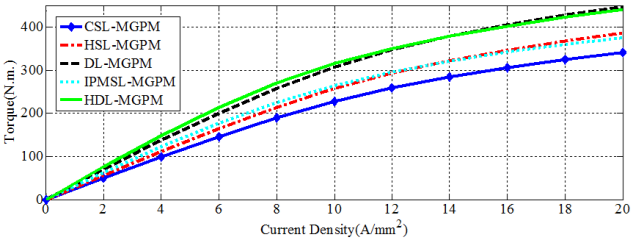

FIGURE 11. Torque-current density waveforms.

the IPMSL-MGPM, the DL-MGPM, the HSL-MGPM, and the CSL-MGPM are 168.9 V, 154 V, 139 V, 125.2 V, and 110.6 V, respectively. As illustrated in Fig. 9(b) the voltage of the proposed structure is higher than others at all speeds.

The torque of the MGPM machines is shown in Figs. 10(a) and 10(b) in equal conditions, such that the 8 A/mm^2 sinusoidal three phase current has 152 Hz frequency, and the outer rotor rotates at 480 rpm. As a result, the structure of HDL-MGPM increases the torque density considerably, which is 42.3%, 26%, 20%, and 5.3% higher than CSL-MGPM, HSL-MGPM, DL-MGPM, and IPM-MGPM, respectively.

As shown in Fig. 11, Owing to the saturation effect of the stator core and slots, the rise in torque was not linear with respect to current density. It is shown that the dramatic decrease in rate of increasing torque owing to higher current density leads to core and slots saturation. Therefore, the current density is selected as 8 A/mm^2 because it is the knee–point of the torque–current curve.

The flux densities of machines with current density 8 A/mm2 are illustrated in Fig.12.

As shown in Fig. 13, the proposed structure increases the effect of the inner rotor on the torque density, more than

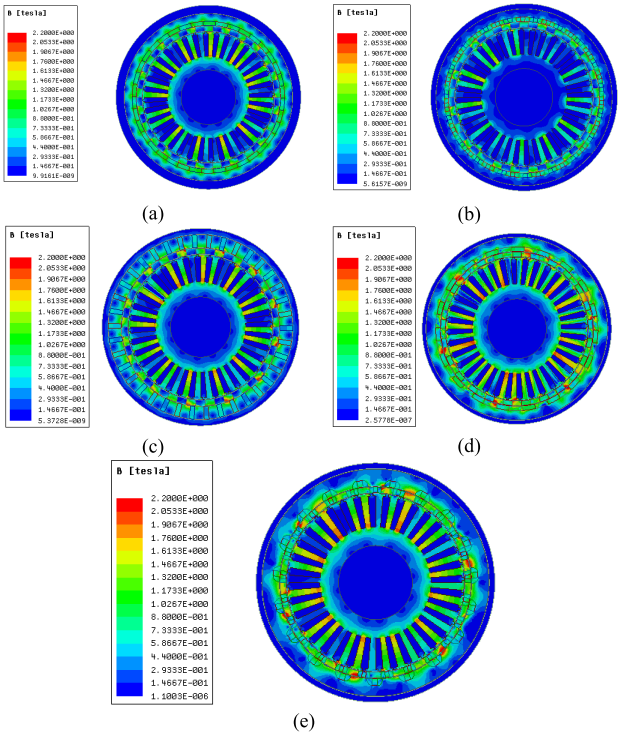

FIGURE 12. The flux densities of machines: (a) CSL-MGPM (b) HSL-MGPM (c) IPMSL-MGPM (d) DL-MGPM (e) HDL-MGPM.

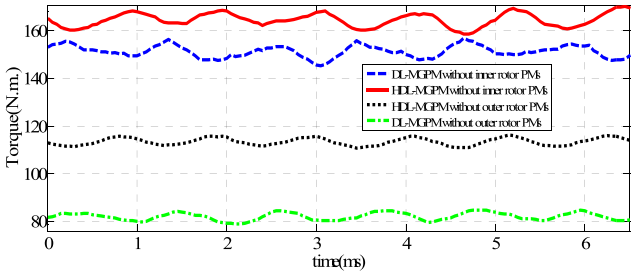

FIGURE 13. Effect of the inner and outer rotor PMs on the electromagnetic torque waveforms.

TABLE 2. Specifications of MGPM Machines.

	CSL-MGPM	HSL-MGPM	IPMSL-MGPM	DL-MGPM	HDL-MGPM
Rated torque (N.m.)	190	215	258	225	275
Current density (A/mm^2)	8				
Rated torque ripple (N.m.)	5	3	10	17.5	12
Torque per PM volume ($KN.m./m^3$)	704.5	798.8	923.5	775.5	1020
Torque per weight (N.m./Kg)	9.23	10.47	12.10	9.55	13.37
Torque Density ($KN.m./m^3$)	59.83	67.83	78.42	65.84	77.3

that by the DL-MGPM, by using Halbach PM arrays in the inner and outer rotor PMs. Therefore, 40% of the torque

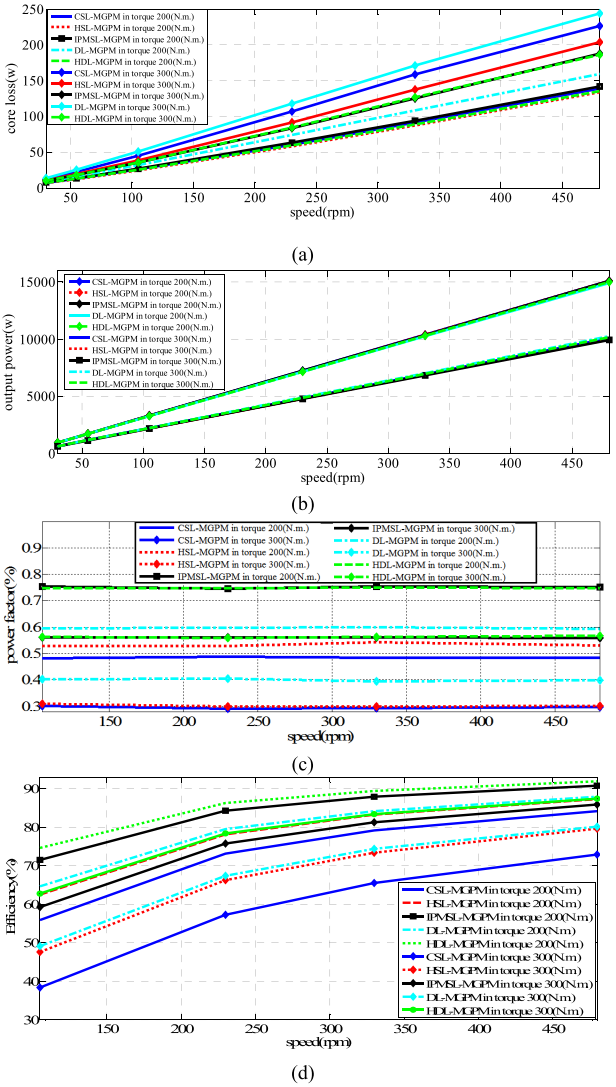

FIGURE 14. Core loss and output power and efficiency and power factor of these machines vs speed.

of the proposed structure is produced by the inner rotor. In the proposed structure, the inner and outer rotor effects are increased by 7.3% and 5.2%, respectively, in comparison with the DL-MGPM.

According to Table 2, the torque ripple of the DL-MGPM is higher compared to other MGPM machines, but the proposed structure reduces the torque ripple in comparison with the DL-MGPM. Furthermore, the torque density of these MGs can be more than 150 kNm/m3, if the current have been increased and the dimensions have been changed.

The core loss and output power and efficiency and power factor of these machines are illustrated in the Fig. 14.

VII. EFFECT OF GEOMETRY PARAMETERS ON THE PROPOSED MGPM MACHINE

The effects of inner and outer rotor thickness and outer and inner rotor PM ratio (D_{PM}/D_{st}) on the torque of the proposed structure are investigated.

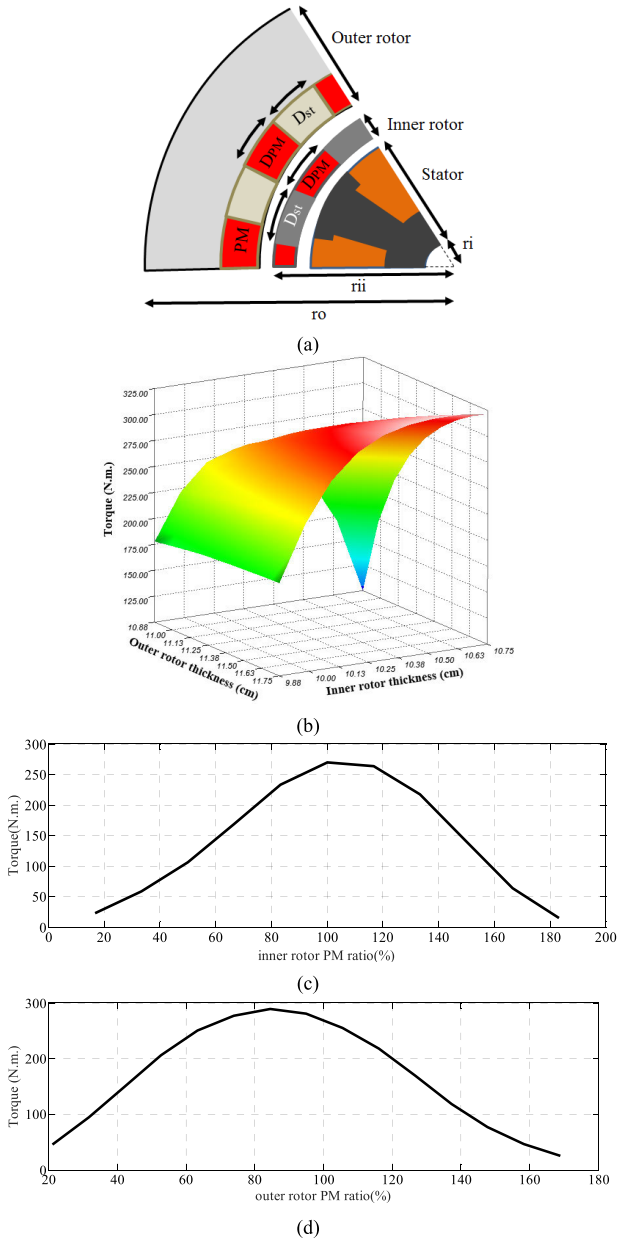

FIGURE 15. Torque of the outer rotor versus the inner and outer rotor thickness, and the PM ratio (D_{PM}/D_{st}).

As shown in Fig. 15(b), by increasing the thickness of inner and outer rotor, the torque of the machine is increased. As shown in Figs. 15(c) and 15(d), in order to create a higher torque in the proposed structure, the ratio of the PMs to the steel pole pieces (D_{PM}/D_{st}) in the inner and outer rotors should be approximately equal (approximately 100%). In Fig. 16, the effect of other geometry parameters on torque of the proposed structure is shown.

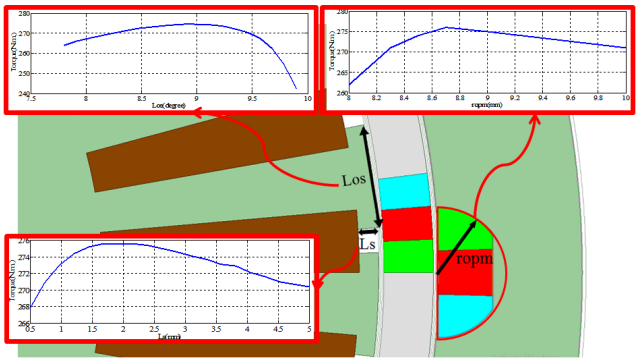

FIGURE 16. Torque of the proposed structure versus the geometry parameters.

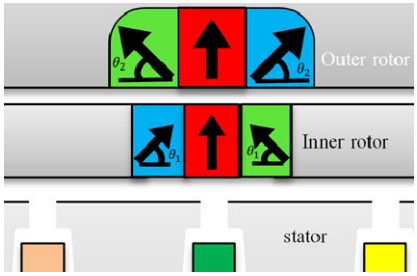

FIGURE 17. Magnetization direction of the Halbach PM array of the inner and outer rotor PMs.

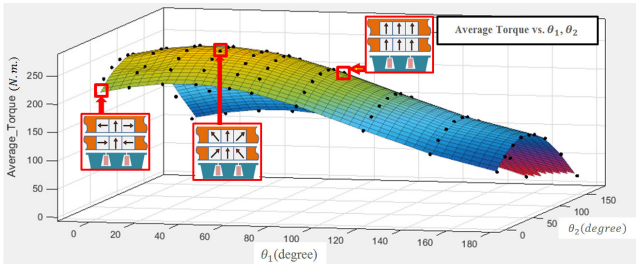

FIGURE 18. Average torque vs Magnetization direction of the Halbach PM array of the inner and outer rotor PMs.

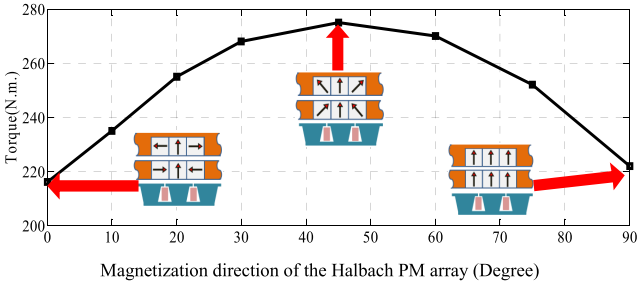

FIGURE 19. Torque-angle waveforms.

VIII. EFFECT OF MAGNETIZATION DIRECTIONS ON THE PROPOSED MGPM MACHINE

Magnetization direction of the Halbach PM array of the inner and outer rotor PMs are shown in Fig. 17. As shown in Figures 18 and 19, by increasing the angle between magnetization direction of PMs and the PM axis from 0 to 45 degree, the average torque is increased. However, by going beyond the 45 degree, the average torque experiences a decline. As illustrated in Fig. 19, it is obvious that 0 degree is the same as the Halbach PM arrays by 2 segments per pole

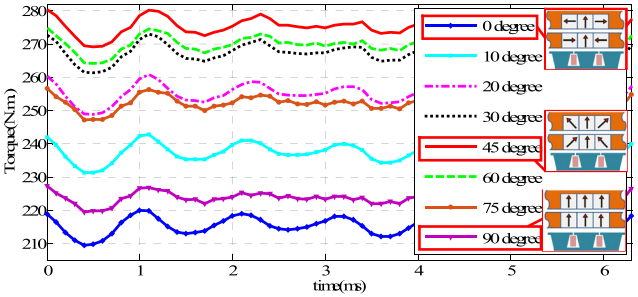

FIGURE 20. Torque vs time characteristic.

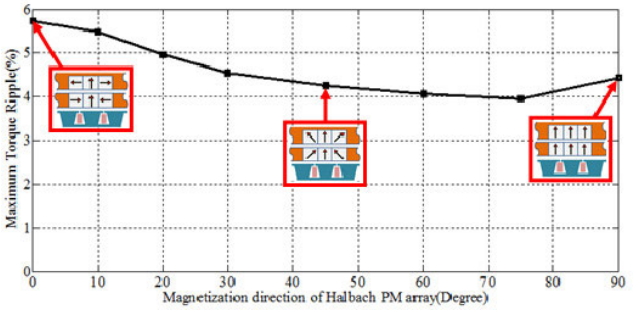

FIGURE 21. Torque ripple-angle waveforms.

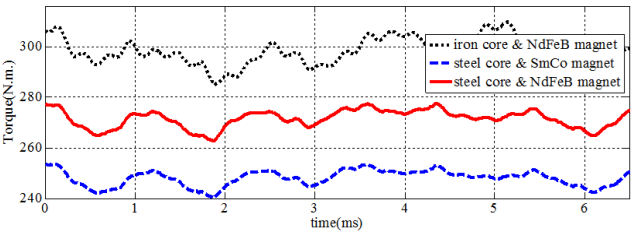

FIGURE 22. Electromagnetic torque curves.

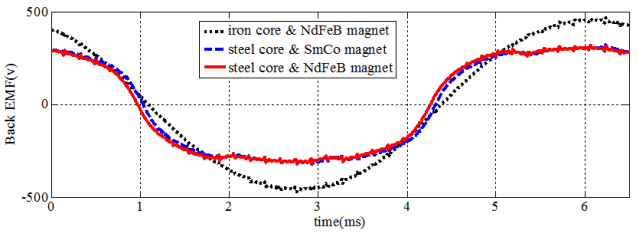

FIGURE 23. Induced back-EMF waveforms.

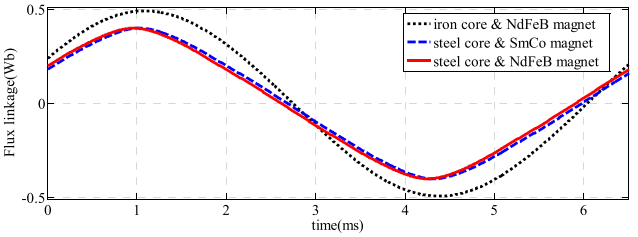

FIGURE 24. Flux linkage waveforms.

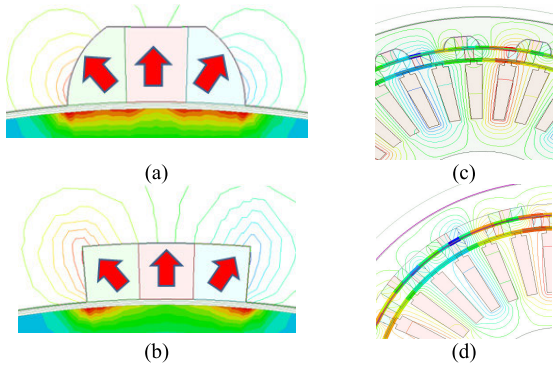

FIGURE 25. Magnetic fluxes of (a) Bread-Loaf-shaped magnet (b) Rectangle-Shaped Magnet (c) HDL-MGPM with Bread-Loaf shaped magnet (d) HDL-MGPM with Rectangle Shaped Magnet.

and 90 degrees is the same as the DL-MGPM. The torque–time curve of the MGPM machines is shown in Fig. 20. It is noted that the $\theta 1$ and $\theta 2$ are supposed to be the same in the Figures 19, 20 and 21.

In the proposed structure, the mentioned angle is selected as 45 degree in order to create the best Halbach PM arrays on the inner and outer rotor PMs. Therefore, as expected the torque of machine via the Halbach PM arrays by 3 segments per pole is greater than that via the Halbach PM arrays by 2 segments per pole, which is shown in Fig. 20. The Halbach PM array by 3 segments per pole is the highest waveform in Fig. 20. Moreover, as shown in Fig. 21, the torque ripple versus angle is approximately constant.

IX. EFFECT OF MATERIALS OF THE LAYERS CORE ON THE PROPOSED MGPM MACHINE

The Fig. 22 can be achieved if the type of the core layer is changed and different types of PMs are used. It is shown that the amplitude of the torque density has increased by 30 N.m. (11%) when the type of the layer is changed from steel to iron. Furthermore, by selecting the iron core instead of steel core, the torque ripple of the machine has increased by 41%, which is a disadvantage of the iron core. Additionally, by changing the type of the PMs from NdFeB to SmCo, the electromagnetic torque is reduced by 8%, and the torque ripple is decreased by 17%.

In addition, as shown in Figs. 23 and 24, the back-EMF voltage is higher when iron is selected as the core layer rather than steel since the flux of the machine is higher.

X. EFFECT OF BREAD-LOAF SHAPED PM IN THE PROPOSED STRUCTURE

The structure of dual-layer increases the torque of the machine considerably, and the torque ripple is increased

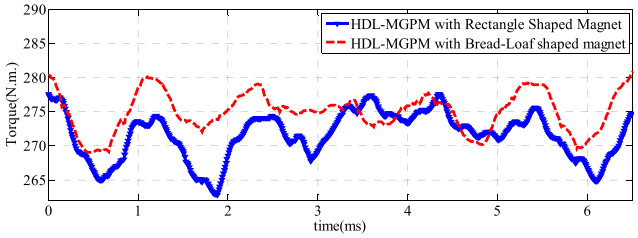

FIGURE 26. Torque of the HDL-MGPM machine.

TABLE 3. Effect Of The Shape Of The Magnet On Torque.

Structure	Torque ripple (%)	Cogging torque (N.m.)
HDL-MGPM with Rectangle Shaped Magnet	5.46	12.665
HDL-MGPM with Bread-Loaf shaped magnet	4.73	8.715

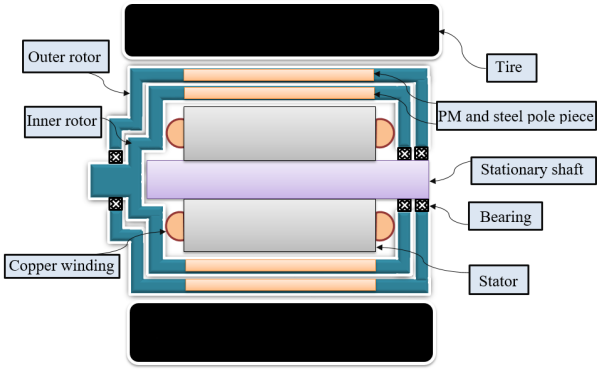

FIGURE 27. Cross section of the proposed MGPM machine.

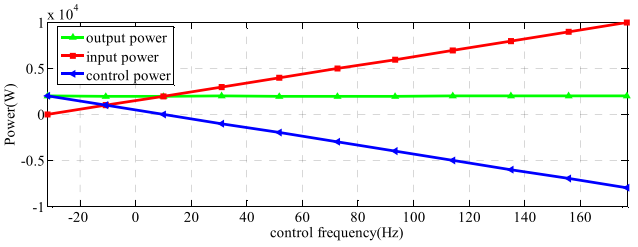

FIGURE 28. Operation of E-CVT.

intrinsically. Subsequently, there is a need for designing a new structure in order to decrease the torque ripple of the machine. Therefore, in the proposed structure, the Bread-Loaf shaped PM is employed on the outer rotor PMs. As shown in Fig. 25, the magnetic fields in the outer air gap adjacent to the outer rotor PMs are augmented in order to enhance the torque density and reduce the torque ripple. Then, the torque of the proposed structure is improved as shown in Fig. 26. Furthermore, the effect of the shape of magnet on torque ripple and cogging torque is shown in Table 3.

XI. ELECTRIC CONTINUOUS VARIABLE TRANSMISSION SYSTEM

Furthermore, the proposed MGPM machine can act as an E-CVT in order to perform the power transmission between the inner and outer rotor and stator continuously. As shown in Fig. 27, this novel structure can be utilized in hybrid electric vehicles instead of planetary gear set and the generator (or motor), which is connected to the sun gear. In this way, the inner and outer rotor can be controlled with the coil current as in (6) and (10). Hence, the gear ratio can be changed by controlling the frequency of the coil current. As shown in Fig. 28, the output power remains constant when the inner rotor speed rises up.

XII. CONCLUSION

MGs have high efficiency, inherent overload protection, and no need for lubrication; however, they suffer from the low torque density. Hence, the significant contribution of this study is the proposal of the novel high torque density MGPM machine structure. Furthermore, the proposed structure reduces the torque ripple and decreases the probability of core saturation. In contrast, some structures have been presented in order to increase the torque density. Hence, it is noteworthy that fair comparison is implemented in this study. Moreover, it is illustrated that the torque of the proposed structure is 42.3%, 26%, 20%, and 5.3% higher than that of the CSL-MGPM, HSL-MGPM, DL-MGPM, and IPM-MGPM, respectively. Thereafter, the effects of some key parameters on the proposed structure performance and the E-CVT operation are investigated.

REFERENCES

[1] Y. Wang, M. Filippini, N. Bianchi, and P. Alotto, "A review on magnetic gears: Topologies, computational models, and design aspects," *IEEE Trans. Ind. Appl.*, vol. 55, no. 5, pp. 4557–4566, Sep. 2019.
[2] P. M. Tlali, R.-J. Wang, and S. Gerber, "Magnetic gear technologies: A review," in *Proc. Int. Conf. Electr. Mach. (ICEM)*, Sep. 2014, pp. 544–550.
[3] H. Polinder, J. A. Ferreira, B. B. Jensen, A. B. Abrahamsen, K. Atallah, and R. A. McMahon, "Trends in wind turbine generator systems," *IEEE J. Emerg. Sel. Topics Power Electron.*, vol. 1, no. 3, pp. 174–185, Sep. 2013.
[4] M. Chen, K. T. Chau, and C. Liu, "Design of a new non-rare-earth magnetic variable gear for hybrid vehicular propulsion system," *IET Elect. Syst. Transp.*, vol. 6, no. 3, pp. 153–162, 2016.
[5] O. Molokanov, P. Dergachev, S. Osipkin, E. Kuznetsova, and P. Kurbatov, "A novel double-rotor planetary magnetic gear," *IEEE Trans. Magn.*, vol. 54, no. 11, pp. 1–5, Nov. 2018.
[6] A. Zaini, N. Niguchi, and K. Hirata, "Continuously variable speed Vernier magnetic gear," *IEEE Trans. Magn.*, vol. 48, no. 11, pp. 3104–3107, Nov. 2012.
[7] M. Filippini, P. Alotto, V. Cirimele, M. Repetto, C. Ragusa, L. Dimauro, and E. Bonisoli, "Magnetic loss analysis in coaxial magnetic gears," *Electronics*, vol. 8, no. 11, p. 1320, Nov. 2019.
[8] Y. Wang, M. Filippini, G. Bacco, and N. Bianchi, "Parametric design and optimization of magnetic gears with differential evolution method," *IEEE Trans. Ind. Appl.*, vol. 55, no. 4, pp. 3445–3452, Jul. 2019.
[9] S. S. Laxminarayan, M. Singh, A. H. Saifee, and A. Mittal, "Design, modeling and simulation of variable speed axial flux permanent magnet wind generator," *Sustain. Energy Technol. Assessments*, vol. 19, pp. 114–124, Feb. 2017.
[10] L. Shah, A. Cruden, and B. W. Williams, "A variable speed magnetic gear box using contra-rotating input shafts," *IEEE Trans. Magn.*, vol. 47, no. 2, pp. 431–438, Feb. 2011.

[11] L. L. Wang, J. X. Shen, P. C. K. Luk, W. Z. Fei, C. F. Wang, and H. Hao, "Development of a magnetic-geared permanent-magnet brushless motor," *IEEE Trans. Magn.*, vol. 45, no. 10, pp. 4578–4581, Oct. 2009.

[12] L. Jian, Z. Deng, Y. Shi, J. Wei, and C. C. Chan, "The mechanism how coaxial magnetic gear transmits magnetic torques between its two rotors: Detailed analysis of torque distribution on modulating ring," *IEEE/ASME Trans. Mechatronics*, vol. 24, no. 2, pp. 763–773, Apr. 2019.

[13] K. Aiso, K. Akatsu, and Y. Aoyama, "A novel reluctance magnetic gear for high-speed motor," *IEEE Trans. Ind. Appl.*, vol. 55, no. 3, pp. 2690–2699, May 2019.

[14] L. Jian, K. T. Chau, Y. Gong, J. Z. Jiang, C. Yu, and W. Li, "Comparison of coaxial magnetic gears with different topologies," *IEEE Trans. Magn.*, vol. 45, no. 10, pp. 4526–4529, Oct. 2009.

[15] A. Grauers, "Efficiency of three wind energy generator systems," *IEEE Trans. Energy Convers.*, vol. 11, no. 3, pp. 650–657, Sep. 1996.

[16] B. Dianati, H. Heydari, and S. A. Afsari, "Analytical computation of air-gap magnetic field in a viable superconductive magnetic gear," *IEEE Trans. Appl. Supercond.*, vol. 26, no. 6, pp. 1–12, Sep. 2016.

[17] L. Jian and K. T. Chau, "A coaxial magnetic gear with Halbach permanent-magnet arrays," *IEEE Trans. Energy Convers.*, vol. 25, no. 2, pp. 319–328, Jun. 2010.

[18] M. Cirolini, A. F. Flores Filho, Y. C. Wu, and D. G. Dorrell, "Design aspects of a reluctance-based magnetic lead screw," *IEEE Trans. Magn.*, vol. 55, no. 7, pp. 1–6, Jul. 2019.

[19] L. Huang, Z. Q. Zhu, J. Feng, S. Guo, J. X. Shi, and W. Chu, "Analysis of stator/rotor pole combinations in variable flux reluctance machines using magnetic gearing effect," *IEEE Trans. Ind. Appl.*, vol. 55, no. 2, pp. 1495–1504, Mar. 2019.

[20] I.-H. Jo, H.-W. Lee, G. Jeong, W.-Y. Ji, and C.-B. Park, "A study on the reduction of cogging torque for the skew of a magnetic geared synchronous motor," *IEEE Trans. Magn.*, vol. 55, no. 2, pp. 1–5, Feb. 2019.

[21] X. Liu, Y. Zhao, Z. Chen, D. Luo, and S. Huang, "Multi-objective robust optimization for a dual-flux-modulator coaxial magnetic gear," *IEEE Trans. Magn.*, vol. 55, no. 7, pp. 1–8, Jul. 2019.

[22] P. Su, W. Hua, Z. Wu, Z. Chen, G. Zhang, and M. Cheng, "Comprehensive comparison of rotor permanent magnet and stator permanent magnet flux-switching machines," *IEEE Trans. Ind. Electron.*, vol. 66, no. 8, pp. 5862–5871, Aug. 2019.

[23] Z. Zeng, Y. Shen, Q. Lu, D. Gerada, B. Wu, X. Huang, and C. Gerada, "Flux-density harmonics analysis of switched-flux permanent magnet machines," *IEEE Trans. Magn.*, vol. 55, no. 6, pp. 1–7, Jun. 2019.

[24] Y. Zhan, L. Ma, K. Wang, H. Zhao, G. Xu, and N. Ding, "Torque analysis of concentric magnetic gear with interconnected flux modulators," *IEEE Trans. Magn.*, vol. 55, no. 6, pp. 1–4, Jun. 2019.

[25] F. Wu and A. M. El-Refaie, "Permanent magnet Vernier machine: A review," *IET Electr. Power Appl.*, vol. 13, no. 2, pp. 127–137, Feb. 2019.

[26] K.-H. Shin, H.-W. Cho, K.-H. Kim, K. Hong, and J.-Y. Choi, "Analytical investigation of the on-load electromagnetic performance of magnetic-geared permanent-magnet machines," *IEEE Trans. Magn.*, vol. 54, no. 11, pp. 1–5, Nov. 2018.

[27] G. Liu, Y. Jiang, J. Ji, Q. Chen, and J. Yang, "Design and analysis of a new fault-tolerant magnetic-geared permanent-magnet motor," *IEEE Trans. Appl. Supercond.*, vol. 24, no. 3, pp. 1–5, Jun. 2014.

[28] P. O. Rasmussen, T. O. Andersen, F. T. Jorgensen, and O. Nielsen, "Development of a high-performance magnetic gear," *IEEE Trans. Ind. Appl.*, vol. 41, no. 3, pp. 764–770, May 2005.

[29] K. K. Uppalapati, W. B. Bomela, J. Z. Bird, M. D. Calvin, and J. D. Wright, "Experimental evaluation of low-speed flux-focusing magnetic gearboxes," *IEEE Trans. Ind. Appl.*, vol. 50, no. 6, pp. 3637–3643, Nov. 2014.

[30] M. B. Kouhshahi, J. Z. Bird, V. M. Acharya, K. Li, M. Calvin, W. Williams, and S. Modaresahmadi, "An axial flux focusing magnetically geared generator for low input speed applications," *IEEE Trans. Ind. Appl.*, vol. 56, no. 1, pp. 138–147, Jan. 2020.

[31] K. Li, S. Modaresahmadi, W. B. Williams, J. Z. Bird, J. D. Wright, and D. Barnett, "Electromagnetic analysis and experimental testing of a flux focusing wind turbine magnetic gearbox," *IEEE Trans. Energy Convers.*, vol. 34, no. 3, pp. 1512–1521, Sep. 2019.

[32] K. K. Uppalapati, M. D. Calvin, J. D. Wright, J. Pitchard, W. B. Williams, and J. Z. Bird, "A magnetic gearbox with an active region torque density of 239 N·m/L," *IEEE Trans. Ind. Appl.*, vol. 54, no. 2, pp. 1331–1338, Mar./Apr. 2018.

[33] K. N. Jenney and S. Pakdelian, "Leakage flux of the trans-rotary magnetic gear," *IEEE Trans. Magn.*, vol. 55, no. 7, pp. 1–8, Jul. 2019.

[34] L. Jing, Z. Huang, J. Chen, and R. Qu, "An asymmetric pole coaxial magnetic gear with unequal Halbach arrays and spoke structure," *IEEE Trans. Appl. Supercond.*, vol. 30, no. 4, pp. 1–5, Jun. 2020.

[35] F. Hu, Y. Zhou, H. Cui, and X. Liu, "Spectrum analysis and optimization of the axial magnetic gear with Halbach permanent magnet arrays," *Energies*, vol. 12, no. 10, p. 2003, May 2019.

[36] M.-S. Sim and J. Ro, "Semi-analytical modeling and analysis of Halbach array," *Energies*, vol. 13, no. 5, p. 1252, Mar. 2020.

[37] R. S. Dragan, R. E. Clark, E. K. Hussain, K. Atallah, and M. Odavic, "Magnetically geared pseudo direct drive for safety critical applications," *IEEE Trans. Ind. Appl.*, vol. 55, no. 2, pp. 1239–1249, Mar. 2019.

[38] S. Niu, T. Sheng, X. Zhao, and X. Zhang, "Operation principle and torque component quantification of short-pitched flux-bidirectional-modulation machine," *IEEE Access*, vol. 7, pp. 136676–136685, 2019.

[39] Y. Wang, S. Niu, and W. Fu, "Sensitivity analysis and optimal design of a dual mechanical port bidirectional flux-modulated machine," *IEEE Trans. Ind. Electron.*, vol. 65, no. 1, pp. 211–220, Jan. 2018.

[40] Q. Wang, S. Niu, and S. Yang, "Design optimization and comparative study of novel magnetic-geared permanent magnet machines," *IEEE Trans. Magn.*, vol. 53, no. 6, pp. 1–4, Jun. 2017.

[41] A. Matthee, R.-J. Wang, C. J. Agenbach, D. N. Els, and M. J. Kamper, "Evaluation of a magnetic gear for air-cooled condenser applications," *IET Electr. Power Appl.*, vol. 12, no. 5, pp. 677–683, 2018.

[42] Z. Song, C. Liu, and H. Zhao, "Investigation on magnetic force of a flux-modulated double-rotor permanent magnet synchronous machine for hybrid electric vehicle," *IEEE Trans. Transp. Electrific.*, vol. 5, no. 4, pp. 1383–1394, Dec. 2019.

[43] C. Tong, M. Wang, P. Zheng, J. Bai, and J. Liu, "Characteristic analysis and functional validation of a brushless flux-modulated double-rotor machine for HEVs," *IEEE Trans. Ind. Electron.*, vol. 66, no. 1, pp. 663–673, Jan. 2019.

[44] H. Zhao, C. Liu, Z. Song, and S. Liu, "A consequent-pole PM magnetic-geared double-rotor machine with flux-weakening ability for hybrid electric vehicle application," *IEEE Trans. Magn.*, vol. 55, no. 7, pp. 1–7, Jul. 2019.

[45] B. McGilton, R. Crozier, A. McDonald, and M. Mueller, "Review of magnetic gear technologies and their applications in marine energy," *IET Renew. Power Gener.*, vol. 12, no. 2, pp. 174–181, Feb. 2018.

[46] M. Zhou, X. Zhang, W. Zhao, J. Ji, and J. Hu, "Influence of magnet shape on the cogging torque of a surface-mounted permanent magnet motor," *Chin. J. Electr. Eng.*, vol. 5, no. 4, pp. 40–50, Dec. 2019.

[47] S. Ruangsinchaiwanich, Z. Q. Zhu, and D. Howe, "Influence of magnet shape on cogging torque and back-emf waveform in permanent magnet machines," in *Proc. Int. Conf. Electr. Mach. Syst.*, vol. 1, 2005, pp. 284–289.

[48] H. Pengfei, J. Shuanbao, W. Yingsan, L. Nan, Z. Qinghu, W. Xingyu, Z. Hao, and S. Fangxu, "A study of third-harmonic shaping in surface-mounted permanent magnet machine with bread-shape magnetic pole," in *Proc. 22nd Int. Conf. Electr. Mach. Syst. (ICEMS)*, Aug. 2019, pp. 1–5.

[49] L. Jing, J. Gong, Z. Huang, T. Ben, and Y. Huang, "A new structure for the magnetic gear," *IEEE Access*, vol. 7, pp. 75550–75555, 2019.

[50] K. Atallah and D. Howe, "A novel high-performance magnetic gear," *IEEE Trans. Magn.*, vol. 37, no. 4, pp. 2844–2846, Jul. 2001.

[51] S. Niu, S. L. Ho, and W. N. Fu, "A novel double-stator double-rotor brushless electrical continuously variable transmission system," *IEEE Trans. Magn.*, vol. 49, no. 7, pp. 3909–3912, Jul. 2013.

[52] L. Wu, R. Qu, D. Li, and Y. Gao, "Power transferring of magnetic-geared permanent magnet machines," in *Proc. IEEE Energy Convers. Congr. Expo. (ECCE)*, Sep. 2016, pp. 1–7.

SOHEIL YOUSEFNEJAD received the B.S. degree in electrical engineering from Shahid Beheshti University, Tehran, Iran, in 2015, and the M.Sc. degree from the Iran University of Science and Technology (IUST), Tehran, in 2018, both in electrical power engineering. He is currently working with the High Voltage and Magnetic Materials Research Center, IUST. His research interests include magnetic gears, electrical drives, and lithium ion battery.

HOSSEIN HEYDARI received the B.S. degree in electrical engineering and the M.Sc. degree in power electronics from Loughborough University, Loughborough, U.K., in 1985 and 1987, respectively, and the Ph.D. degree in transformer core losses from the University of Wales, Cardiff, U.K., in 1993. Following graduation, he joined the Iran University of Science and Technology (IUST), Tehran, Iran, as an Academic Member (Lecturer) of the Electrical Power Group, and also appointed as the Director of the High Voltage and Magnetic Materials Research Center. He is currently with the Center of Excellence for Power System Automation and Operation, IUST. His research interests include EMC considerations in power systems, magnetic gears, fault current limiters, and applied superconductivity in power systems.

KAN AKATSU received B.S., M.S., and Ph.D. degrees in electrical engineering from Yokohama National University, Yokohama, Japan, in 1995, 1997, and 2000, respectively. He joined the Nissan Research Center, Yokosuka, Japan, in 2000, where he contributed to the design and analysis of the new concept permanent magnet machines. In 2003, he joined the Department of Electrical and Electric Engineering, Tokyo University of Agriculture and Technology, Tokyo, Japan, as an Assistant Professor. In 2009, he was an Associate Professor and a Full Professor with the Shibaura Institute of Technology, Tokyo. Since October 2019, he has been a Professor with Yokohama National University. He is a Committee Member in IEEJ-IAS and the Chair of International Affairs of IEEJ-IAS. From 2005 to 2007, he received the JSPS Postdoctoral Fellowship for Research Abroad as a Visiting Professor with Wisconsin Electric Machines and Power Electronics Consortium (WEMPEC), University of Wisconsin-Madison.

JONGSUK RO received the B.S. degree in mechanical engineering from the Hanyang University, Seoul, South Korea, in 2001, and the Ph.D. degree in electrical engineering from the Seoul National University (SNU), Seoul, in 2008.

In 2014, he was with the University of Bath, Bath, U.K., as an Academic Visitor. From 2013 to 2016, he worked with the Brain Korea 21 Plus, SNU, as a BK Assistant Professor. He conducted research with the Electrical Energy Conversion System Research Division, Korea Electrical Engineering and Science Research Institute, as a Researcher, in 2013. From 2012 to 2013, he was with the Brain Korea 21 Information Technology, SNU, as a Postdoctoral Fellow. He conducted research with the Research and Development Center, Samsung Electronics, as a Senior Engineer, from 2008 to 2012. He is currently an Associate Professor with the School of Electrical and Electronics Engineering and an Adjunct Professor with the Department of Intelligent Energy and Industry (BK4), Chung-Ang University, Seoul. His research interest includes the analysis and optimal design of next-generation electrical machines using smart materials, such as electromagnet, piezoelectric, and magnetic shape memory alloy.